BIOCHEMISTRY
including biophysical chemistry & molecular biology

Article

pubs.acs.org/biochemistry

Characterization of an Aldolase–Dehydrogenase Complex from the Cholesterol Degradation Pathway of *Mycobacterium tuberculosis*

Jason Carere, Sarah E. McKenna, Matthew S. Kimber, and Stephen Y. K. Seah*

Department of Molecular and Cellular Biology, University of Guelph, Guelph, Ontario, Canada N1G 2W1

Supporting Information

ABSTRACT: HsaF and HsaG are an aldolase and dehydrogenase from the cholesterol degradation pathway of *Mycobacterium tuberculosis*. HsaF could be heterologously expressed and purified as a soluble dimer, but the enzyme was inactive in the absence of HsaG. HsaF catalyzes the aldol cleavage of 4-hydroxy-2-oxoacids to produce pyruvate and an aldehyde. The enzyme requires divalent metals for activity, with a preference for Mn^{2+}. The K_m values for 4-hydroxy-2-oxoacids were about 20-fold lower than observed for the aldolase homologue, BphI from the polychlorinated biphenyl degradation pathway. Acetaldehyde and propionaldehyde were channeled directly to the dehydrogenase, HsaG, without export to the bulk solvent where they were transformed to acyl-CoA in an NAD^+ and coenzyme A dependent reaction. HsaG is able to utilize aldehydes up to five carbons in length as substrates, with similar catalytic efficiencies. The HsaF–HsaG complex was crystallized and its structure was determined to a resolution of 1.93 Å. Substitution of serine 41 in HsaG with isoleucine or aspartate resulted in about 35-fold increase in K_m for CoA but only 4-fold increase in K_m dephospho-CoA, suggesting that this residue interacts with the 3′-ribose phosphate of CoA. A second protein annotated as a 4-hydroxy-2-oxopentanoic acid aldolase in *M. tuberculosis* (MhpE, Rv3469c) was expressed and purified, but was found to lack aldolase activity. Instead this enzyme was found to possess oxaloacetate decarboxylase activity, consistent with the conservation (with the 4-hydroxy-2-oxoacid aldolases) of residues involved in pyruvate enolate stabilization.

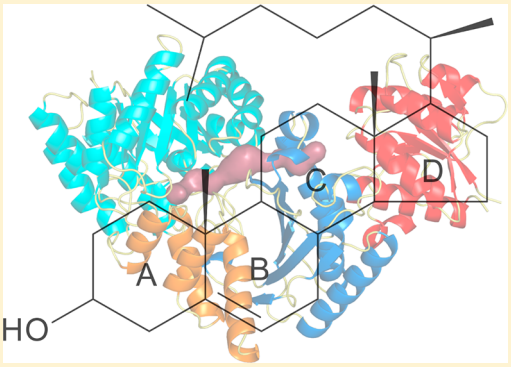

Mycobacterium tuberculosis is the causative agent of tuberculosis (TB), a bacterial infection that kills nearly 2 million people annually.[1] During infection, *M. tuberculosis* survives within the phagosome compartment of macrophages for long periods of time due to its ability to inhibit phagosome-lysosome fusion. Cholesterol, derived from the host's membrane and lipid bodies within macrophages, has been implicated as an important carbon source for *M. tuberculosis* within the nutrient poor macrophage phagosome-like compartment. Specifically, cholesterol catabolism leads to formation of the central metabolites pyruvate and propionyl-CoA. The latter can be transformed into tricarboxylic acid cycle metabolites, or unique cell wall lipids important for virulence in this bacterium. Cholesterol uptake and degradation have been shown to be essential for intracellular growth and survival of *M. tuberculosis* in animal models,[1,2] and the disruption of certain genes encoding enzymes in the cholesterol degradation pathway leads to reduced virulence and, in some cases, accumulation of toxic dead-end steroid metabolites that are detrimental to the survival of the bacterium growing on cholesterol.[3−5]

Although the ability of diverse bacteria to degrade steroids[6,7] has been known for some time, the exact catabolic pathway and its associated genes/enzymes are still not fully elucidated. Comparisons of the *M. tuberculosis* genome to those of other steroid degrading bacteria, such as the related actinomycete, *Rhodococcus jostii* RHA1[8] has allowed the identification of a gene cluster encoding putative cholesterol degrading enzymes. Cholesterol degradation can be divided into two parts: side chain degradation and the degradation of the steroid rings. The latter is thought to proceed through a pathway analogous to the bacterial *meta*-cleavage pathway of aromatics, such as phenols and polychlorinated biphenyls (PCBs).

The degradation of diverse aromatic compounds via the *meta*-cleavage pathway generally leads to the formation of the common intermediate, 4-hydroxy-2-oxopentanoate, as exemplified by the *bph* pathway responsible for biphenyl/polychlorinated biphenyl (PCBs) degradation. A divalent metal dependent pyruvate aldolase then catalyzes a retro aldol cleavage of this intermediate, generating pyruvate and acetaldehyde.[9] Acetaldehyde is converted to acetyl-CoA by an acylating aldehyde dehydrogenase that forms a complex with the aldolase. Various aldolase-dehydrogenase complexes including BphI–BphJ from the biphenyl degradation pathway, DmpG–DmpF from the phenol degradation pathway, and TTHB246–TTHB247 from *Thermus thermophilus* have been characterized. Structural and biochemical studies have shown that the acetaldehyde product of the aldolase is not released in the bulk solvent, but rather travels to the aldehyde dehydrogenase via a molecular tunnel connecting the active sites of the two

Received: March 18, 2013
Revised: April 23, 2013
Published: April 24, 2013

Scheme 1. Cholesterol Degradation Pathway in *M. tuberculosis* Showing the Formation of 4-Hydroxy-2-oxohexanoate (HOHA) from Rings A and B[a]

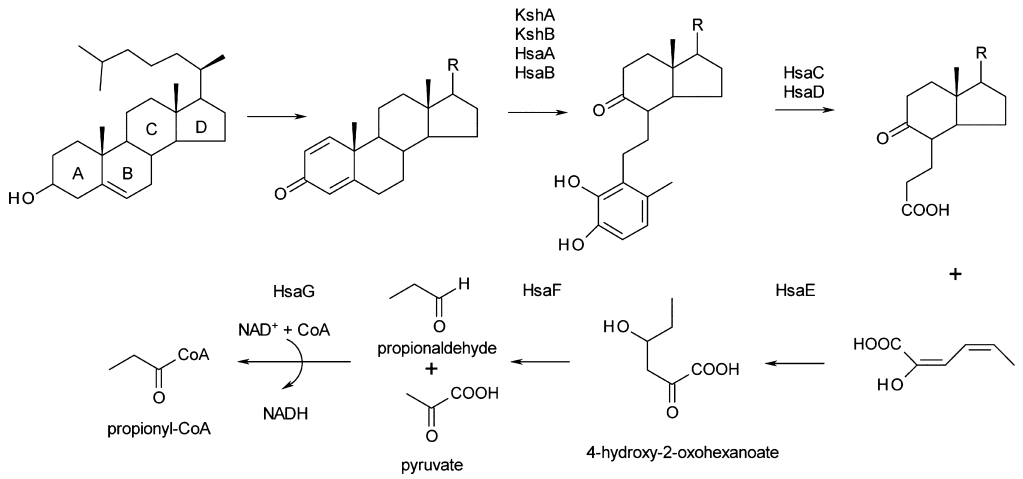

[a]HOHA is converted to pyruvate and propionyl CoA by the aldolase HsaF and the acetaldehyde dehydrogenase, HsaG. The pathway for cholesterol side chain degradation is not shown (depicted as an R in the figure).

enzymes.[10,11] This process, known as substrate channeling, enables the sequestration of the labile and toxic aldehyde, while ensuring that unwanted products from competing cellular reactions are minimized.[12−14] Analysis of the aldolase and dehydrogenase genes across the genomes of diverse aromatic-degrading bacteria reveals that they are generally adjacent to each other, with the aldehyde dehydrogenase preceding the aldolase gene in an operon. With the exception of a few rare cases, attempts to express each gene separately in a heterologous host such as in *Escherichia coli* leads to formation of inclusion bodies or unstable proteins.[9,11,15]

The aldolase−dehydrogenase complexes from steroid degradation pathways have not been previously purified and characterized.[16] Phylogenetic analysis of protein sequences reveals that these aldolases and dehydrogenases (HsaF and HsaG encoded by Rv3534c and Rv3535c respectively in *M. tuberculosis* H37Rv) form a clade in the phylogenetic tree (Clade I) distinct from the aldolases and dehydrogenases from other aromatic degradation pathways.[17] HsaF−HsaG differs from homologous enzymes from other aromatic degradation pathways in that steroid degradation yields 4-hydroxy-2-oxohexanoate; this molecule is one carbon longer than 4-hydroxy-2-oxopentanoate, the common metabolite from other aromatic degradation pathways (such as PCBs). In the second step, aldol cleavage of 4-hydroxy-2-oxohexanoate produces propionaldehyde rather than acetaldehyde, so both enzymes act on substrates larger by one methylene group (Scheme 1).

Here we describe the heterologous expression, purification, and characterization of HsaF-HsaG from *M. tuberculosis* H37Rv. The crystal structure, steady-state kinetic parameters, and substrate specificity of HsaF−HsaG were determined and compared with aldolase−dehydrogenase complexes from other aromatic degradation pathways. We also analyze an additional putative aldolase encoded by Rv3469c (annotated as MhpE based on putative homology with the *E. coli* 4-hydroxy-2-oxopentanoate aldolase) and show that this protein lacks 4-hydroxy-2-oxoacid aldolase activity but does possess oxaloacetate decarboxylase activity. Detailed sequence analysis reveals that this protein and its orthologs differ in key catalytic site residues, allowing them to be differentiated from the 4-hydroxy-2-oxoacid aldolases.

EXPERIMENTAL APPROACH

Chemicals. All aldehydes, NAD^+, NADH, oxaloacetate, pyruvate, L-lactate dehydrogenase (LDH, rabbit muscle), aldehyde dehydrogenase (*Saccharomyces cerevisiae*), alcohol dehydrogenase (*Saccharomyces cerevisiae*), and 2-keto-3-deoxy-octonate (KDO) were from Sigma-Aldrich (Oakville, ON). Ni-NTA Superflow resin was obtained from Qiagen (Mississauga, ON). 4(*S*)- and 4(*R*)-Hydroxy-2-oxopentanoate and 4-hydroxy-2-oxohexanoate were synthesized using BphI according to previously described methods.[18,19] The *M. tuberculosis* H37Rv genomic DNA was a gift from Dr. Marcel Behr (McGill University, QC). 4-Hydroxy-4-methyl-2-oxoglutarate (HMG) and 4-carboxy-4-hydroxy-2-oxoadipate (CHA) were synthesized chemically using pyruvate and oxaloacetate as previously described.[20] Enantiomerically pure HOHA was synthesized using wild-type BphI. All other chemicals were analytical grade and were obtained from Sigma-Aldrich or Fisher Scientific (Nepean, ON).

DNA Manipulation. DNA was purified, digested, and ligated using standard protocols. Genes were amplified from *M. tuberculosis* H37Rv genomic DNA by PCR using the primers shown in Table S1. The amplified fragments were ligated into pCR-Blunt II-TOPO (Invitrogen) and transformed into *E. coli* DH5α. As there is an internal *NdeI* cleavage site within the *Rv3469c* gene, a silent mutation was introduced by site-directed mutagenesis using the modified Quickchange (Stratagene) method.[21] Positive clones were sent to Guelph Molecular Supercenter (University of Guelph) for confirmation of the sequence. The *Rv3469c*, *hsaGF*, and *hsaG* genes were then transferred into pET28a by insertion in the NdeI and *Hin*dIII sites and *hsaF* in pBTLT7 [9] for expression tests in *E. coli*. The genes from the pET28a plasmid constructs were then digested with *NcoI* and *Hin*dIII and inserted into similarly digested *p*TIP QC1.[22] This plasmid was then transformed into *Rhodococcus jostii* RHA1 as described by Shao et al.[23]

Protein Expression and Purification. *R. jostii* RHA1 containing the *hsaGF p*TIP QC1-His construct was propagated at 30 °C in 4 L of Luria−Bertani medium supplemented with 25 μg/mL chloramphenicol. When the optical density of the culture at 600 nm reached 0.6, the expression of HsaF−HsaG

dx.doi.org/10.1021/bi400351h | *Biochemistry* 2013, 52, 3502−3511

was induced with 1 μg/mL of thiostrepton. Upon induction, the cells were kept at 30 °C for 24 h and harvested by centrifugation at 9605*g* for 8 min.

The cells were resuspended in 20 mM HEPES pH 8.5 and lysed by passage through a French press five times at a pressure of 25000 psi. Cellular debris was removed by three successive centrifugations at 39191*g* for 10 min each. The clarified lysate was then passed though a 0.45 μm filter, and HsaF−HsaG was purified as in Baker et al.[9] HsaF and HsaG were expressed and purified similarly with the exception that their $(His)_6$ tags were not cleaved. The *Rv3469c* gene product was expressed and purified similarly to HsaF−HsaG except that cultures were induced at an optical density of 0.4, the poly-His tag was not cleaved, and dithiothreitol (DTT) was not added prior to storage.

Sodium dodecyl sulfate-polyacrylamide gel electrophoresis was performed, and gels were stained with Coomassie Blue to assess purity. Purified enzyme was aliquoted and stored in 20 mM HEPES buffer, pH 8.5 with 10 mM DTT at −80 °C. The concentration of enzyme was determined using the Bradford method.[24] The native molecular mass of purified HsaF, HsaG, the gene product of *Rv3439c* and HsaF−HsaG complex were estimated using gel filtration on a HiLoad 26/60 Superdex 200 column (GE Healthcare). Chromatography was performed at 25 °C in 20 mM HEPES buffer, pH 7.5, containing 150 mM NaCl, at a flow rate of 2 mL/min. Molecular masses were calculated from elution volumes using a standard curve obtained with a standard kit for molecular weights (Sigma).

Dehydrogenase Activity Assays. Substrate specificity of the dehydrogenase was determined using 0.4 mM NAD^+, 0.4 mM coenzyme A unless otherwise stated, and aldehyde concentrations were varied from at least 0.1 K_m to 5 K_m. Concentrations of aldehyde stocks were determined by measuring the stoichiometric oxidation of NADH using alcohol dehydrogenase. Cofactor specificities were determined under similar conditions in which the acetaldehyde concentrations were held at 100 mM, and concentrations of NAD^+ and CoA concentration were varied between 0.1 K_m and 5 K_m, in the absence of DTT.

Aldolase Activity Assays. Aldol cleavage activity was determined continuously or discontinuously by coupling the production of pyruvate to LDH and monitoring the oxidation of NADH.[9] All assays were performed at least in duplicate, at 25 °C in a total volume of 1 mL using a Varian Cary 3 spectrophotometer with a thermojacketted cuvette holder. Standard continuous assays contained 0.4 mM NADH, 1 mM $MnCl_2$ and 19.2 Units LDH in 100 mM HEPES buffer (pH 8.0). The concentration of 4-hydroxy-2-oxoacids was varied from 0.1 K_m to 10 K_m. Oxidation of NADH was monitored continuously at 340 nm with the extinction coefficient taken as 6200 $M^{-1}\cdot cm^{-1}$. To assess the activity of HsaF in the absence of NADH, a discontinuous assay was utilized. Assay mixtures contained 1 mM $MnCl_2$, 250 μm HOPA or HOHA, and 80 μg of HsaF−HsaG in 100 mM HEPES buffer (pH 8.0). After 10 min, the reaction was quenched with 20 mM EDTA (pH 8.5) and 0.4 mM NADH. The amount of pyruvate produced was measured by an end point assay using LDH.

Decarboxylase Activity Assay. Oxaloacetate decarboxylase activity was determined continuously by coupling the production of pyruvate to LDH and monitoring the oxidation of NADH.[5] All assays were performed at least in duplicate, at 25 °C in a total volume of 1 mL using a Varian Cary 3 spectrophotometer with a thermojacketted cuvette holder. Standard continuous assays contained 0.4 mM NADH, 1 mM $MnCl_2$, and 19.2 units LDH in 100 mM HEPES buffer (pH 8.0). The concentration of oxaloacetate was varied from 0.1 K_m to 10 K_m. Oxidation of NADH was monitored continuously at 340 nm, with the extinction coefficient taken as 6200 $M^{-1}\cdot cm^{-1}$.

Metal Specificity. The metal ion specificity of HsaF was determined by incubating 20 μg of HsaF−HsaG with EDTA for 20 min and then removing the EDTA by dilution in Chelex treated buffer. All assay components were treated with Chelex, and a standard aldolase assay was performed. 0.1 mM and 1 mM concentrations of various metal chlorides were tested.

Test of Substrate Channeling. The amount of aldehyde channeled directly from the aldolase to the dehydrogenase without export to the bulk solvent was assessed using an enzyme competition assay previously described.[10] Unless otherwise stated, assays contained NAD^+ at a concentration of at least 5 K_m, coenzyme A at a concentration of least 3 K_m, 25 μM substrate, 1 mM $MnCl_2$, and 10 μg of HsaF-HsaG with 20 U yeast aldehyde dehydrogenase (ALDH), which converts aldehydes to acids and reduces NAD^+ to NADH. Reactions were quenched after 5 min with 24 μL of 3 N HCl and centrifuged for 3 min at 21000*g* to pellet the denatured enzyme. A 500 μL aliquot of the reaction mixture was subjected to high performance liquid chromatography (HPLC) using an ÄKTA Explorer 100 (Amersham Pharmacia Biotech, Baie d'Urfe, QC) equipped with a HyPURITY C18 column (Thermo Scientific). The sample was eluted with 50 mM sodium phosphate (pH 5.3)/acetonitrile; (47:3). The channeling efficiency was calculated by comparing the concentration of acyl-CoA produced (determined using HPLC) to the concentration of 4-hydroxy-2-oxoacid utilized by the aldolase, based on the amount of NADH produced as previously described.[10]

Dissociation Constant of NAD^+. The dissociation constant of NAD^+ was assessed by tryptophan fluorescence quenching upon NAD^+ binding. Experiments were completed using a PTI QuantaMaster C-61 steady-state fluorimeter (Photon Technology International, London, ON), with a 1 nm bandwidth for excitation (λ_{ex} = 290 nm) and a 2 nm bandwidth for emission (λ_{em} = 333 nm). Titrations were completed in 500 μL of 20 mM HEPES pH 8.5 at 25 °C with 100 μg of enzyme. NAD^+ was added stepwise to the enzyme mixture. Fluorescence intensity was corrected for dilution factors, and the dissociation constant was calculated by fitting to eq 2, which describes binding to one site:

$$\left(\frac{\Delta F}{F_o} \times 100\right) = \frac{(\Delta F_{max}/F_o \times 100) \times [S]}{K_d + [S]} \quad (2)$$

where $(\Delta F/F_0 \times 100)$ is the percent fluorescence quenching (percent change in fluorescence relative to the initial value, F_o) following addition of substrate at a concentration [S]. Fitting was carried out using nonlinear regression using GraphPad Prism.

Activation of HsaF by HsaG. Activation of HsaF by HsaG was determined by titrating HsaG into a solution of HsaF. Each enzyme was purified separately and quantified. 1.15 nmol of HsaF was incubated with various quantities of HsaG in 134 μL of 20 mM HEPES pH 8.5 and 20 mM DTT for 2 h. After incubation, a standard aldolase assay was performed to assess the activity of HsaF.

Crystallization Conditions and Structure Solution. HsaF−HsaG crystals were grown using the sitting drop method

at 25 °C, using 2 μL of reservoir solution consisting of 18% PEG 4000, 0.2 M $MgCl_2$, 0.1 M Tris pH 8.5, 10% glycerol, and 10 mM sodium oxalate, and 2 μL of 10 mg/mL of HsaF−HsaG. The crystals were soaked in the following solution 13% PEG 4000, 0.2 M $MgCl_2$, 0.1 M Tris pH 8.5, 50% vol/vol glycerol, and 10 mM sodium oxalate for 5 min, and flash frozen in liquid nitrogen. The data was collected to 1.93 Å at the Canadian Light Source, Canadian Macromolecular Crystallography Facility (08ID-1) and processed using XDS.[25,26] Crystals were of the monoclinic spacegroup, *C*2, with unit cell dimensions of a = 69.69 Å, b = 142.69 Å, c = 148.17 Å, and β = 95.08°. Molecular replacement was performed in Phaser[27] searching with a homology model of HsaF−HsaG derived from the structure DmpG−DmpF from *Pseudomonas putida* CF600 (PDB code: 1NVM).[28] After an initial structure was determined using autobuild in PHENIX, the structure was rebuilt in Coot[29] and further refined with PHENIX refine.[28] The crystal consists of a heterotetramer of two aldolases with residues 1−3 and 342−346 (343 in chain C) missing and two dehydrogenases with residues 1, 2 and 299−303 missing. Table S2 contains data collection and final refinement statistics. Structure figures were generated in PyMol.[30]

RESULTS

Expression and Purification of Recombinant Proteins. The genes *hsaG* and *hsaF*, encoding the dehydrogenase and aldolase of the cholesterol degradation pathway, are adjacent within the genome of *M. tuberculosis* and are partially overlapping. The individual genes were PCR amplified from *M. tuberculosis* genomic DNA and separately inserted into two compatible *E. coli* plasmids, pBTLT7 and pET28a, respectively. Since the dehydrogenase, HsaG, was expressed with an N-terminal histidine-tag encoded by the pET28a vector, the HsaF−HsaG complex could be copurified by Ni^{2+}-NTA chromatography. However, the yields of purified protein complex were very low with about 200−400 μg of protein purified per liter of recombinant *E. coli* culture. In an attempt to improve protein yields, we transferred the *hsaF*, *hsaG*, and *hsaGF* genes into the *Rhodococcal*−*E. coli* shuttle plasmid pTIPQC1, for expression of the genes in *R. jostii* RHA1, an actinomyete that has been previously used successfully to overexpress other *M. tuberculosis* cholesterol degrading genes.[31] The individual enzymes and enzyme complex were purified by Ni^{2+}-NTA column chromatography. The yields of the HsaF, HsaG, and HsaF−HsaG complex were about 2−3 mg per liter of recombinant *R. jostii* RHA1 culture, a significant improvement from the yields obtained from the *E. coli* expression system. Purified proteins were subjected to SDS-PAGE, and their migration in the gel was consistent with the calculated molecular masses of 36.4 kDa and 32 kDa for HsaF and HsaG, respectively. The native molecular masses of the enzymes complex was determined by gel filtration to be 159 kDa, consistent with a quaternary structure of two aldolase and two dehydrogenase subunits. The individually purified HsaF and HsaG elute at times consistent with them being a dimer (native molecular mass of 67 kDa) and monomer (native molecular mass of 38 kDa), respectively.

Similar to *hsaF* and *hsaG*, the putative *mhpE* was expressed in recombinant *R. jostii* RHA1 as an N-terminally histidine tagged product (Supporting Information, Figure S1). Approximately 2 mg of protein was purified from each liter of culture. The native molecular mass of the enzyme was determined by gel filtration to be 68 kDa, consistent with a homodimeric quartenary structure, similar to that observed for HsaF.

Steady State Kinetic Analysis of HsaF. Although HsaF can be expressed independently of HsaG, the purified HsaF has no detectable aldolase activity toward 4-hydroxy-2-oxopentanoate (HOPA) or 4-hydroxy-2-oxohexanoate (HOHA) (<0.0001 s^{-1}). The enzyme also lacks oxaloacetate decarboxylase activity; this reaction, like the aldolase reaction, proceeds via a pyruvate enolate intermediate and is commonly seen in metal-dependent pyruvate aldolases. Aldolase activity is, however, observed when HsaF is expressed and copurified with HsaG. The specific activity of HsaF in the HsaF−HsaG complex was tested using HOHA as a substrate and with various divalent metal ions at a concentration of 0.1 and 1 mM (Table 1). The specific activity of HsaF was highest with Mn^{2+} followed by Co^{2+} and Ni^{2+}. There is no detectable aldolase activity when HsaF-HsaG is incubated in the presence of Cd^{2+}, Zn^{2+}, or Cu^{2+} (<0.0001 s^{-1}). Using Mn^{2+} as cofactor, HsaF had similar kinetic parameters for HOPA and HOHA enantiomers synthesized using wild-type BphI (Table 2). The former compound has been determined to be the 4(S) enantiomer.[18] Conversely, HsaF is not active toward the opposite enantiomer of HOPA synthesized using the BphI variant Y290F/L87W.[19]

Table 1. Metal Ion Specificity of HsaF[a]

	relative activity %	
metal ion	0.1 mM metal chloride salts	1 mM metal chloride salts
Mn^{2+}	89.5	100
Ni^{2+}	21.1	76
Co^{2+}	30	59.5
Mg^{2+}	26.9	35.1
Ca^{2+}	3.6	15.4
Cd^{2+}	–	–
Zn^{2+}	–	–
Cu^{2+}	–	–

[a]The activity obtained with 1 mM Mn^{2+} is taken as 100%. Assay contained 20 μg of enzyme either 0.1 or 1 mM metal chloride salt, 2 mM 4-hydroxy-2-oxohexanoate, 0.4 mM NADH, 19.2 units of LDH in 100 mM HEPES buffer (pH 8.0) with a total volume of 1 mL. (−) no detectable activity (<0.0001 s^{-1})

Table 2. Steady State Kinetic Parameters of HsaF[a]

substrate	K_m (μM)	k_{cat} (s^{-1})	k_{cat}/K_m (× 10^4 M^{-1} s^{-1})
4-hydroxy-2-oxopentanoate	4.4 ± 0.5	0.41 ± 0.01	9.31 ± 1.08
4-hydroxy-2-oxohexanoate	4.8 ± 0.6	0.38 ± 0.01	7.91 ± 1.01

[a]Aldolase assays were performed at 25 °C and contained 0.4 mM NADH, 1 mM $MnCl_2$ and 19.2 Units LDH in 100 mM HEPES buffer (pH 8.0).

Allosteric Activation of HsaF by HsaG. Although HsaF expressed and purified independently from HsaG has no detectable activity, preincubating the two purified proteins together effectively restored aldolase activity. The specific activity of HsaF in response to increasing concentrations of HsaG was found to follow a sigmoidal saturation curve (Figure 1).

Previous work with the BphI−BphJ complex showed that the aldolase activity is enhanced by about 5-fold in the presence of

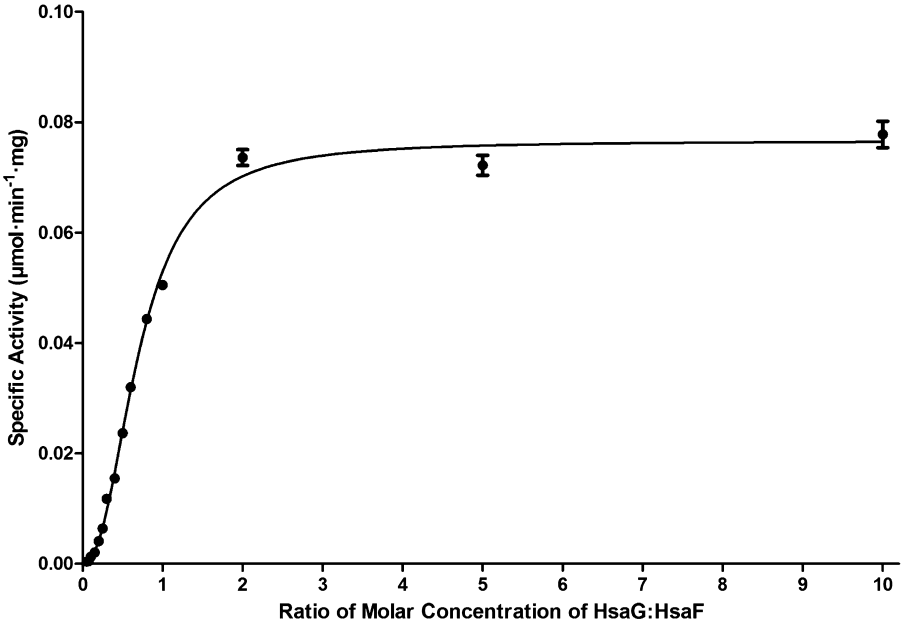

Figure 1. Activity of HsaF when preincubated with varying concentrations of HsaG. 1.15 nmol of HsaF was incubated with various quantities of HsaG in 134 μL of 20 mM HEPES pH 8.5 and 20 mM DTT for 2 h. Subsequently, aldolase activity was determined at 25 °C and assays contained 0.4 mM NADH, 1 mM $MnCl_2$, and 19.2 U LDH in 100 mM HEPES buffer (pH 8.0) The data was fitted with an allosteric sigmoidal model (Using GraphPad Prism).

the dehydrogenase cofactor, NADH. A similar allosteric activation also occurs in the HsaF−HsaG complex; however, at a concentration of 0.4 mM NADH, the level of activation is less than 1.5-fold (0.25 ± 0.01 μmol·min^{-1}·mg versus 0.33 ± 0.01 μmol·min^{-1}·mg).

Steady State Kinetic Analysis of the putative MhpE. The putative MhpE encoded by *Rv3469c* was found to lack any detectable aldolase activity with HOPA or HOHA (<0.0001 s^{-1}), even when incubated with HsaG. No activity was detected with other 4-hydroxy-2-oxoacids, namely, 2-oxo-3-deoxyoctonate (KDO), 4-hydroxy-4-methyl-2-oxoglutarate (HMG), and 4-carboxy-4-hydroxy-2-oxoadipate (CHA). The protein does however exhibit oxaloacetate decarboxylase activity, with a K_m value of 3.07 ± 0.07 mM, k_{cat} value of 0.49 ± 0.04 s^{-1}, and a catalytic efficiency (k_{cat}/K_m) of 1.60 ± 0.14 × 10^2 M^{-1} s^{-1}. This activity is abolished upon incubation of the enzyme with Chelex and EDTA, indicating that the oxaloacetate decarboxylase activity is metal ion dependent. The activity of the apoenzyme can be restored upon addition of excess Mn^{2+} in the assay.

Substrate Specificity of HsaG. Kinetic parameters for the aldehyde dehydrogenase activity of HsaG were investigated for both the HsaF−HsaG complex (Table 3) and for HsaG purified alone (Table 4). Unlike HsaF, HsaG is active both in the presence and absence of its partner enzyme. However, in the absence of HsaF, HsaG exhibits significant substrate inhibition, with a K_i of 50 ± 7 mM for acetaldehyde and 63 ± 6 mM for propionaldehyde. Substrate specificity for HsaG was relatively broad, with linear aldehyde substrates of up to five carbon atoms being utilized with similar catalytic efficiencies (Table 3). In terms of cofactor specificity, the enzyme preferred NAD^+ over $NADP^+$, but exhibited a similar specificity for dephospho-coenzyme A as for coenzyme A. The dissociation constant of NAD^+, determined by tryptophan fluorescence quenching titration, was 1.7 ± 0.2 μM.

Substrate Channeling. HsaF-HsaG was able to channel acetaldehyde and propionaldehyde from the aldol cleavage of HOPA and HOHA, respectively, with similar efficiencies (99 ± 3% and 98 ± 1%). Substrate channeling was completely abrogated by substitution of Gly-322 (which lines the tunnel linking the aldolase and dehydrogenase catalytic sites) with phenylalanine.

Table 3. Steady State Kinetic Parameters of HsaG when in Complex with HsaF with Various Substrates and Cofactors[a]

substrate/cofactor	$K_{m,app}$ (mM)	$k_{cat,\ app}$ (s^{-1})	$k_{cat}/K_{m,\ app}$ (× 10^2 M^{-1}s^{-1})
acetaldehyde[a]	18 ± 2	9.4 ± 0.3	5.2 ± 0.6
propionaldehyde[a]	15 ± 1	11.1 ± 0.2	7.4 ± 0.5
butyrlaldehyde[a]	10.6 ± 0.8	7.3 ± 0.2	6.9 ± 0.6
isobutyrlaldehyde[a]	10 ± 1	5.8 ± 0.3	5.8 ± 0.6
pentaldehyde[a]	20 ± 3	7.8 ± 0.5	3.9 ± 0.6
coenzyme A[b]	0.040 ± 0.003	9.6 ± 0.2	2400 ± 180
NAD^{+}[c]	0.022 ± 0.002	7.6 ± 0.2	3450 ± 330
$NADP^{+}$[c]	1.4 ± 0.1	3.4 ± 0.1	25 ± 2

[a]Assays were performed at 25 °C and contained 0.4 mM NAD^+ and 0.4 mM coenzyme A in 100 mM HEPES buffer (pH 8.0). [b]Assays were performed at 25 °C and contained 100 mM propionaldehyde, and 0.4 mM NAD^+ in 100 mM HEPES buffer (pH 8.0) [c]Assays were performed at 25 °C and contained 100 mM propionaldehyde, and 0.4 mM CoA in 100 mM HEPES buffer (pH 8.0)

Crystal Structure of HsaF−HsaG. HsaF−HsaG (PDB ID: 4JN6) structure was determined at 1.93 Å using a homology model of HsaF−HsaG based on the DmpF−DmpG (1NVM) as model for molecular replacement. The structure contains two aldolase and two dehydrogenase protomers, organized as the biological heterotetramer in the asymmetric unit. The two aldolases (chains A and C) form a dimer, with the two dehydrogenase molecules (Chains B and D) attaching to the periphery of the dimer, to form an elongated BACD complex (Figure 2A). Analysis using the DALI server[32] revealed a root-mean-square deviation (RMSD) of 1.1 Å between the structure of HsaF and DmpG, the corresponding aldolase from the

dx.doi.org/10.1021/bi400351h | *Biochemistry* 2013, 52, 3502−3511

Table 4. Steady State Kinetics of HsaG in the Absence of HsaF

cofactor/substrate	$K_{m,app}$ (mM)	$k_{cat,\ app}$ (s^{-1})	$k_{cat}/K_{m,\ app}$ ($\times 10^3\ M^{-1}\ s^{-1}$)	K_i (mM)
acetaldehyde[a]	21.3 ± 2.7	19.0 ± 1.5	0.89 ± 0.13	50 ± 7
propionaldehyde[a]	12.4 ± 1.1	23.8 ± 0.7	1.93 ± 0.18	63 ± 6
coenzyme A[b]	0.415 ± 0.053	15 ± 1	36 ± 5.2	
NAD^+[c]	0.022 ± 0.004	3.9 ± 0.2	177 ± 33	

[a]Assays were performed at 25 °C and contained 0.4 mM NAD^+ and 1.5 mM coenzyme A in 100 mM HEPES buffer (pH 8.0). [b]Assays were performed at 25 °C and contained 100 mM propionaldehyde, and 0.4 mM NAD^+ in 100 mM HEPES buffer (pH 8.0) [c]Assays were performed at 25 °C and contained 100 mM propionaldehyde, and 1.5 mM CoA in 100 mM HEPES buffer (pH 8.0)

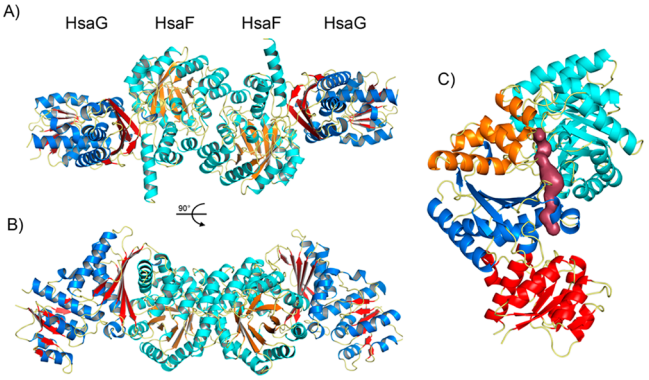

Figure 2. Structure of HsaF–HsaG (A) HsaF–HsaG is organized as a heterotetramer. The HsaF aldolase domains (helices cyan and strands orange) form a homodimer. Each aldolase has an HsaG dehydrogenase (helices blue and strands red) bound to its periphery. (B) Heterotetramer rotated 90° along the 2-fold axis. (C) Tunnel running from the active site of the aldolase to the dehydrogenase as determined by Mole 2.0 [34] is shown in raspberry. Aldolase TIM barrel is shown in cyan, communication domain is shown in orange, dehydrogenase dimerization domain is in blue and Rossmann fold is in red. Images were generated in PyMOL.[30]

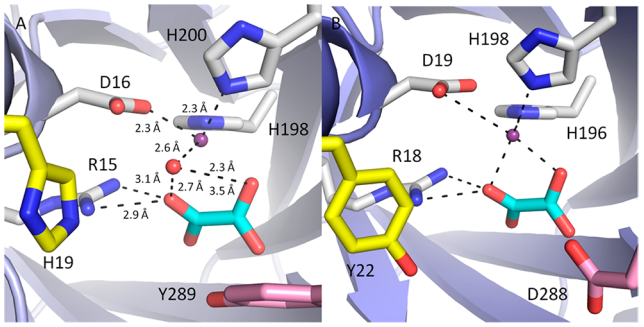

Figure 3. Homology model of Rv3469c superimposed on HsaF. (A) Active site of HsaF with oxalate, a pyruvate enolate analogue, bound. (B) Homology model of the product of *Rv3469c* superimposed on HsaF. The arginine residue (Arg-18), that stabilizes the intermediate and residues which interact with the metal ligands, is conserved between the enzymes (white). The catalytic histidine (His-19; yellow) in HsaF and tyrosine in the active site (Tyr-289 pink) are not conserved and are substituted with tyrosine and aspartate respectively in the gene product of *Rv3469c*. The residues conserved are critical to decarboxylation activity, while the residues which are not conserved are involved with aldolase function. The homology model was produced by SWISS-MODEL;[41] the two proteins share 27% identity and 43% similarity.

phenol degradation pathway of *P. putida* CF600. The dehydrogenases HsaG and DmpF superpose less well, with an RMSD of 1.6–2.2 Å depending on which pair of chains is compared. This variability reflects the domain motion associated with NAD binding in a subset of the DmpF chains; the HsaG apo-structure most closely resembles of DmpF protomer where NAD is not bound. Despite this close global resemblance, the two structures do differ significantly in the organization of the extended loop of the dehydrogenase that interacts with the aldolase (residues 252–268 in DmpF and 248–257 in HsaG) (Figure S2). In DmpF, this region forms a short β-hairpin (residues 258–260 in DmpF); the corresponding loop in HsaG is nine residues shorter and instead forms a short 3_{10} helical motif that packs against a different motif in the aldolase structure.

The HsaF–HsaG complex was cocrystallized with Mn^{2+} and the pyruvate enolate analogue, oxalate, and clear electron density was observed for both ligands in the active site of the aldolase, HsaF. The Mn^{2+} ion is ligated by two histidine residues (His-198 and His-200), two metal bound water molecules and the carboxyl oxygen atoms of oxalate. The oxalate carboxylate group is also bound by the guanidinium group of Arg-15 (Figure 3A). The catalytic site also contains the conserved histidine residue His-19, as well as a structurally conserved water molecule; the analogous groups were previously found to function as the catalytic base and acid in the homologous BphI, and are invariant in HsaF and DmpG.[33]

The active sites of HsaF and HsaG are connected by a tunnel. Analysis using MOLE 2.0[34] (Figure 2B) indicates that the tunnel is approximately 20 Å in length, beginning at Tyr-289 of the aldolase and ending at the entrance of the dehydrogenase active site. While most of the tunnel has a radius of approximately 2.5 Å, a bottleneck 1.3 Å wide is located adjacent to residues Gly-321 and Gly-322 of the aldolase. In HsaG, Ile-167, Ile-191, and Leu-193 line the exit of the tunnel; however, in DmpF, the leucine residue is replaced with a methionine. Superimposition of the HsaG and DmpF structures shows that leucine and methionine occupy approximately the same space, though the methionine methylene group extends further into the catalytic pocket in DmpF.

HsaG contains two domains, a Rossmann fold domain and a dimerization domain, that mediate interactions with the aldolase. The catalytic site is located in a cleft between the domains, and previous work on DmpG-DmpF showed that NAD^+ binding is accompanied by movement of the Rossmann fold domain and closure of the catalytic cleft.[11] In the HsaF structure, the domains are in an open conformation which closely resembles the NAD^+-free DmpG conformation. Locally elevated atomic displacement parameters (ADP), as well as domain fitting by translation/vibration/screw ADP models, indicate that the Rossmann fold domain undergoes an appreciable degree of hinge-bending in the apo structure. Unlike DmpG, the thiol of the catalytic cysteine that forms a

dx.doi.org/10.1021/bi400351h | *Biochemistry* 2013, 52, 3502–3511

thioacyl intermediate with the aldehyde substrate (Cys-127) adopts only one conformation.

HsaG is also structurally related to glycerladehyde-3-phosphate dehydrogenase, aspartate semialdehyde dehydrogenase, and methylmalonyl-CoA reductase.[35−37] The latter, like HsaG, utilizes the Rossmann fold to bind the nicotinamide cofactor and coenzyme A alternately in its reaction mechanism, although it utilizes $NADP^+$ rather than NAD^+ as a cofactor. Although the adenine ribose of $NADP^+$ and coenzyme A both contain a phosphate, the difference in positions of the phosphates (2′ in $NADP^+$ and 3′ in coenzyme A) requires a repositioning of the ribose moiety for the phosphates of the two cofactors to bind in a similar position in the enzyme. This change in position causes the α and β phosphates of the $NADP^+$ to shift toward the catalytic cysteine resulting in the α phosphate of $NADP^+$ binding in the same position as the β phosphate of CoA. The movement of the α and β phosphates and ribose allow for the adenine ring and the ribose phosphates in the two cofactors to bind in a similar position in the protein forming hydrogen bonds with the hydroxyl of a serine residue (Ser-43) in methylmalonyl CoA reductase. Unfortunately, electron density maps derived from crystals grown in the presence of 20 mM coenzyme A, soaked with 20 mM NAD^+ or soaked with coenzyme A showed no evidence for cofactor binding. Instead, coenzyme A was modeled in HsaG by superimposing the adenine ribose with the NAD^+ in the crystal structure DmpF. There is an analogous serine (Ser-41) in HsaG that may mediate similar interactions with the adenine phosphate of coenzyme A (Figure 4B). Ser-41 is ∼4.3 Å away from the predicted position of the 3′ hydroxyl of the ribose ring of NAD^+ (Figure 4A), and it appears that, unlike in methylmalonyl CoA reductase, there is little space to reorient the adenine ribose and the α and β phosphates, potentially accounting for the lower specificity of the HsaG for $NADP^+$ than NAD^+ in contrast to methylmalonyl CoA reductase.

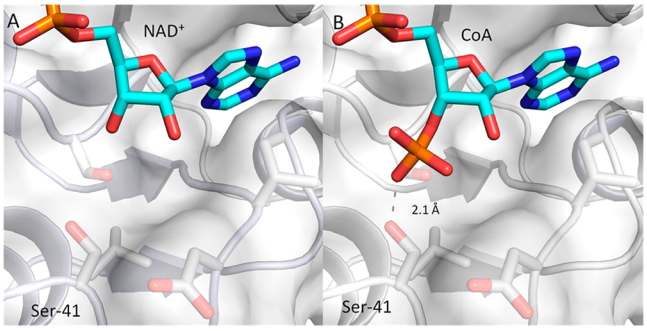

Figure 4. Interaction of Ser-41 with modeled CoA and NAD^+. (A) NAD^+ was positioned in the HsaG structure by superposition with NAD^+ bound DmpG. (B) Proximity of 3′-phosphate of modeled coenzyme A to Ser-41 side chain. The adeninosine moiety is assumed to not shift significantly, and the phosphate was positioned to minimize clashes with the Ser-41 containing loop. Because the loop containing Ser-41 clashes with the phosphate in this position, it is likely required to undergo remodelling upon CoA binding in order to accommodate the phosphate group.

Analysis of the Sequence Relationship between the Putative MhpE and HsaF. It was determined that although arginine (Arg-15) and two metal binding histidine residues (His-198 and His-200) found in HsaF are conserved in the gene product of *Rv3469c*, the putative MhpE lacks the histidine (His-19 in HsaF) that has been previously implicated for base abstraction of the 4-OH group of 4-hydroxy-2-oxoacids, and a tyrosine (Tyr-289) conserved in HOPA aldolases that helps mediate stereospecificity and gating of substrate channeling (Figure 3B); instead the corresponding positions are occupied by phenylalanine and aspartate in MphE. In addition, the C-terminal domain which mediates interactions with the dehydrogenase including forming the tunnel linking the active sites of the aldolase−dehydrogenase complex is missing in the putative MhpE. Orthologs of the putative MhpE found in other *Mycobacterium* species, such as *M. canettii* CIPT 140010059 (95% sequence identity), are also misannotated as 4-hydroxy-2-oxopentanoate aldolases. In these *Mycobacterium* species, the related genes co-operonic with genes encoding proteins homologous to dTDP-glucose 4,6-dehydratase, and to the catalytic subunit of acetolactate synthase. There are no genes with clear homology to aldehyde dehydrogenases in the immediate genomic vicinity. More distant homologues of MphE are found in the archaea *Nitrosopumilus maritimus* SCM1 and *Methanocorpusculum labreanum* Z (sequence similarities of 47% to the gene product of *Rv3469c*; Figure S3). Like the Mycobacterial enzymes, these proteins contain the catalytic residues required for pyruvate enolate formation and stabilization but lack the catalytic base required for aldolase activity. It is therefore likely that these archeal gene products also possess oxaloacetate decarboxylase activity despite having a different genomic context as the *Mycobacterial* genes (Figure S4).

Role of Ser-41 in Coenzyme A Binding. Ser-41 is proposed to interact with the 3′ ribose phosphate group on the coenzyme A (Figure 4B). When Ser-41 was substituted with alanine or aspartate, the specificity constant (k_{cat}/K_m) for coenzyme A was reduced between 3 and 4 orders of magnitude (Table 5). While the k_{cat} value for dephospho-CoA (which lacks the ribose phosphate) was also reduced in the two variants, the $K_{m,app}$ was similar to that of wild-type enzyme. The specificity constant for dephospho coenzyme A in the variants was therefore comparatively less reduced: 44- and 360-fold for the S41D and S41I variants, respectively.

Table 5. Steady State Kinetics of HsaG Variants[a]

enzyme	cofactor	$K_{m,app}$ (μM)	$k_{cat,\ app}$ (s^{-1})	$k_{cat}/K_{m,\ app}$ ($\times 10^4\ M^{-1}\ s^{-1}$)
WT	coenzyme A	40 ± 3	9.6 ± 0.2	24.0 ± 1.8
	dephospho-CoA	13 ± 1	9.7 ± 0.4	74.6 ± 6.5
S41I	coenzyme A	1475 ± 190	0.054 ± 0.004	0.0036 ± 0.0005
	dephospho-CoA	64 ± 6	0.131 ± 0.005	0.205 ± 0.021
S41D	coenzyme A	1525 ± 244	0.16 ± 0.01	0.0105 ± 0.0018
	dephospho-CoA	49 ± 5	0.83 ± 0.03	1.69 ± 0.18

[a]Assays were performed at 25 °C and contained 100 mM propionaldehyde, and 0.4 mM NAD^+ in 100 mM HEPES buffer (pH 8.0).

dx.doi.org/10.1021/bi400351h | *Biochemistry* 2013, 52, 3502−3511

DISCUSSION

The gene product of *Rv3469c* was successfully purified and determined to form a soluble dimer. However, there are no genes encoding a potential partner aldehyde dehydrogenase located in its vicinity in the *M. tuberculosis* genome. The putative MhpE has OAA decarboxylases activity but lacks any detectable aldolase activity with the substrates attempted to date. Sequence analysis reveals that the putative MhpE lacks the catalytic histidine important for C4-OH proton abstraction in the aldolase reaction, which accounts for its lack of 4-hydroxy-2-oxoacid aldolase activity. Instead, this histidine is replaced with tyrosine. However, the metal cofactor ligands and the positively charged arginine residue previously implicated for stabilization of the pyruvate enolate intermediate are conserved between HsaF and the putative MhpE. Since oxaloacetate decarboxylase proceeds through a pyruvate enolate intermediate, it is not surprising that the gene product of *Rv3469c* possess this activity. These results showed that Rv3469c and its orthologs are not 4-hydroxy-2-oxopentanoate aldolases, and these genes are misannotated in a number of *Mycobacterium* genomes. Although it is unclear whether the OAA decarboxylase activity is the physiological or secondary activity, the fact that the gene is contiguous with a gene encoding the large catalytic subunits of acetohydroxy acid synthase (which catalyzes the transformation of two pyruvate molecules to form acetolactate and carbon dioxide) suggests that the OAA decarboxylase activity that forms pyruvate may be the physiologically relevant activity.

HsaF, HsaG, and the HsaF−HsaG complex were successfully expressed and purified from recombinant *R. jostii* RHA1. However, HsaF proved inactive by itself, and formation of a complex with HsaG appears to be required in order to induce a catalytically active conformation. This arrangement is likely adaptive, preventing the deleterious formation and release of toxic aldehydes in the absence of the partner dehydrogenase. Tryptophan synthase, another enzyme that exhibits substrate channeling, behaves in an analogous manner, where complex formation leads to a 1−2 order of magnitude increase in the activities of the α and β subunits.[38] However, unlike the HsaF/HsaG system, the α and β subunits of tryptophan synthase retain significant if reduced activity when not in complex. The ortholog of HsaF from the thermophile *Thermus thermophilus* (TTHB246 49% sequence identity to HsaF) is, on the other hand, active without the partner dehydrogenase (TTHB247), and complex formation has a negligible effect on the k_{cat} value for 4-hydroxy-2-oxopentanoate aldolase activity.[17]

Similar to BphI, but unlike TTHB246 which prefers Co^{2+} as cofactor, HsaF had the highest activity with Mn^{2+} as a metal cofactor. HsaF exhibits approximately 20-fold lower K_m values for 4-hydroxy-2-oxoacids when compared to TTHB246 and BphI.[9,17] The k_{cat} values for these substrates are of the same order of magnitude to those determined for TTHB246 but are about 10-fold lower than BphI. Interestingly, the dehydrogenase HsaG has similar kinetic parameters for aldehydes of 2−5 carbon atoms in length. This contrasts with the BphJ dehydrogenase, where the specificity constant for butyraldehyde is about half that for acetaldehyde or propionaldehyde, while the K_m value for pentaldehyde was too high to be determined. Previously, it was determined that the alkyl chain of aldehyde substrates extend toward the back of the active site of BphJ in proximity to Ile-195 (Ile-191 in HsaG).[39] Substitution of Ile-195 with larger tryptophan and phenylalanine residues led to reduced specificity toward long chain aldehydes in BphJ. A comparison of the crystal structure of HsaG and DmpF reveals that Met-198 in DmpG extends further into the catalytic pocket than the equivalent Leu-193 in HsaG, and occupies multiple conformations, reducing the available space for the distal end of longer chain aldehyde substrates. Paradoxically, inspection of the structure of HsaG and comparison with the BphJ sequence shows that all amino acids lining the catalytic pocket are identical, meaning that the ability of HsaG to utilize longer chain aldehydes more efficiently does not simply arise because HsaG is lined with less bulky side chains. Possibly the answer to this paradox lies in the protein dynamics, where longer alkyl chains may be able to partially occupy the substrate tunnel with a lower energetic penalty.

HsaF−HsaG was able to channel acetaldehyde and propionaldehyde from the aldolase to the dehydrogenase with more than 90% efficiency. Similar to other orthologs, there appears to be a bottleneck in the tunnel linking the active site, lined by glycine residues.[10] Substitution of one of these residues, Gly-322, to the slightly bulkier alanine residue in HsaF blocks aldehyde channeling. BphI and the *T. thermophilus* aldolase homologues were shown to be activated by 5.1- and 2-fold, respectively, in the presence of dehydrogenase cofactors.[17] In comparison, the activity of HsaF in the enzyme complex is only activated 1.3-fold in the presence of NADH.

One intriguing difference in the structures of HsaG and DmpF lies in the organization of an extended loop in the oligomerization domain. In both structures, this loop forms extensive interactions with a conserved region in the partner aldolase, but they contact distinct sites, and use very different contacts. The loop in DmpF is longer and forms a two-stranded mini-sheet that interacts with both the main body of DmpF and DmpG with extensive hydrophobic contacts. The contacts made by the HsaG loop are less extensive and more polar. Sequence alignments and homology modeling have previously suggested that the ortholog BphJ, and other members of its clade, lack this loop entirely.[17] An intriguing possibility is that these loops play a role in stabilizing the aldolase/dehydrogenase interface, and possibly communicating the presence of NAD^+ in the dehydrogenase catalytic site to the aldolase.

It was previously postulated, based on hydrogen−deuterium exchange mass spectrometry analysis, that NAD^+ and CoA share a common binding site in DmpF.[40] Both NAD^+ and CoA have an ADP-ribose moiety, but in CoA the 3′ hydroxyl of the ribose ring is phosphorylated. Assuming the ADP-ribose group of both cofactors bind in the same position, phosphate binding may require a reorganization of the loop containing Ser-42, both because these residues are close enough to form a van der Waal clash and because there are no hydrogen bond donating groups suitably positioned to make favorable interactions with the phosphate. The energetic cost to reorganize this loop would then be offset by energy from favorable interactions with the 3′ phosphate of CoA. Indeed, the $K_{m,app}$ value for dephospho-CoA is slightly less than CoA, suggesting that the considerable potential binding energy inherent in phosphate binding is being diverted into an energetically costly reorganization. The significantly increased $K_{m,app}$ of $NADP^+$ compared to NAD^+ indicates that the phosphate of $NADP^+$ is not properly positioned to make any favorable interactions, and therefore is energetically disfavored by a rearrangement required simply to avoid steric clashes. Wild-type HsaF-HsaG are able to utilize CoA and dephospho-CoA with similar specificity; however the

S41D and S41I variants show considerably reduced efficiencies with CoA (about 2000−6000-fold reduction) compared with dephospho-CoA (44- to 360-fold reduction). Indeed, the $K_{m,app}$ values for dephospho-CoA are similar for the variants and wild-type enzyme. This suggests that Ser-41 plays an important role in binding the 3′ phosphate of the CoA. While difficult to prove without direct structural evidence, the close proximity of Ser-41 to the ribose would suggest that the role of this residue may be as much to help stabilize this loop in an alternative conformation that clears sufficient space for phosphate binding, as to form favorable interactions with the phosphate.

In conclusion, HsaF and HsaG differ from previously characterized aldolase−dehydrogenase complexes from other aromatic pathways in terms of its substrate specificity, degree of allosteric activation, and solubility of the aldolase. Like its distant homologue methylmalonyl-CoA reductase, HsaG contains an equivalent serine residue that we propose interacts with the 3′ phosphate of CoA adenine ribose. However, the difference in specificities for NAD^+ and $NADP^+$ in the evolutionarily related methylmalonyl-CoA reductase and HsaG indicates that this residue is not the molecular determinant for nicotinamide coenzyme discrimination.

■ ASSOCIATED CONTENT

Supporting Information

Table S1. Primers used for amplification of *M. tuberculosis* genes. Introduced *NdeI* and *Hin*dIII cleavage sites are underlined.

Table S2. Data collection, model refinement and final structure statistics for HsaF-HsaG.

Figure S1. SDS-PAGE gel of purified HsaF-HsaG, HsaF, HsaG, and Rv3469c.

Figure S2. Variable length loops on the dehydrogenases.

Figure S3. Sequence alignment of 4-hydroxy-2-oxoacid aldolases with protein orthologs of Rv3469c.

Figure S4. Genetic map of Rv3469c and homologues. This material is available free of charge via the Internet at http://pubs.acs.org.

■ AUTHOR INFORMATION

Corresponding Author

*E-mail: sseah@uoguelph.ca. Phone: 519-824-4120 Ext 56750. Fax: 519-837-1802.

Funding

This research is supported by National Science and Engineering Research Council of Canada (NSERC) Grant 238284 (to S.S.).

Notes

The authors declare no competing financial interest.

■ ACKNOWLEDGMENTS

This research is supported by an operating grant from the National Science and Engineering Research Council of Canada (NSERC) Grants (238284-01 to S.Y.K.S., and 327280 to M.S.K.). J.C and S.M. are recipients of an Ontario Graduate Scholarship and USRA studentship respectively. The authors thank the staff from the Canadian Macromolecular Crystallography Facility for their assistance in data collection.

■ ABBREVIATIONS USED

ALDH, aldehyde dehydrogenase; EDTA, ethylenedinitrilotetraacetic acid; HEPES, 4-(2-hydroxyethyl)-1-piperazinepropanesulfonic acid; HOPA, 4-hydroxy-2-oxopentanoate; HOHA, 4-hydroxy-2-oxohexanoate; LDH, L-lactate dehydrogenase; PEG, polyethylene glycol; HMG, 4-hydroxy-4-methyl-2-oxoglutarate; CHA, 4-carboxy-4-hydroxy-2-oxoadipate; KDO, 2-keto-3-deoxyoctonate

■ REFERENCES

(1) Nesbitt, N. M., Yang, X., Fontan, P., Kolesnikova, I., Smith, I., Sampson, N. S., and Dubnau, E. (2010) A thiolase of Mycobacterium tuberculosis is required for virulence and production of androstenedione and androstadienedione from cholesterol. *Infect. Immun. 78*, 275−282.

(2) Pandey, A. K., and Sassetti, C. M. (2008) Mycobacterial persistence requires the utilization of host cholesterol. *Proc. Natl. Acad. Sci. U. S. A. 105*, 4376−4380.

(3) Yam, K. C., D'Angelo, I., Kalscheuer, R., Zhu, H., Wang, J. X., Snieckus, V., Ly, L. H., Converse, P. J., Jacobs, W. R., Jr., Strynadka, N., and Eltis, L. D. (2009) Studies of a ring-cleaving dioxygenase illuminate the role of cholesterol metabolism in the pathogenesis of *Mycobacterium tuberculosis*. *PLoS Pathog. 5*, e1000344.

(4) Chang, J. C., Harik, N. S., Liao, R. P., and Sherman, D. R. (2007) Identification of Mycobacterial genes that alter growth and pathology in macrophages and in mice. *J. Infect. Dis. 196*, 788−795.

(5) Chang, J. C., Miner, M. D., Pandey, A. K., Gill, W. P., Harik, N. S., Sassetti, C. M., and Sherman, D. R. (2009) igr Genes and Mycobacterium tuberculosis cholesterol metabolism. *J. Bacteriol. 191*, 5232−5239.

(6) Marsheck, W. J., Kraychy, S., and Muir, R. D. (1972) Microbial degradation of sterols. *Appl. Microbiol. 23*, 72−77.

(7) Drzyzga, O., Fernandez de las Heras, L., Morales, V., Navarro Llorens, J. M., and Perera, J. (2011) Cholesterol degradation by Gordonia cholesterolivorans. *Appl. Environ. Microbiol. 77*, 4802−4810.

(8) Van der Geize, R., Yam, K., Heuser, T., Wilbrink, M. H., Hara, H., Anderton, M. C., Sim, E., Dijkhuizen, L., Davies, J. E., Mohn, W. W., and Eltis, L. D. (2007) A gene cluster encoding cholesterol catabolism in a soil actinomycete provides insight into Mycobacterium tuberculosis survival in macrophages. *Proc. Natl. Acad. Sci. U. S. A. 104*, 1947−1952.

(9) Baker, P., Pan, D., Carere, J., Rossi, A., Wang, W., and Seah, S. Y. (2009) Characterization of an aldolase-dehydrogenase complex that exhibits substrate channeling in the polychlorinated biphenyls degradation pathway. *Biochemistry 48*, 6551−6558.

(10) Carere, J., Baker, P., and Seah, S. Y. (2011) Investigating the Molecular Determinants for Substrate Channeling in BphI-BphJ, an Aldolase-Dehydrogenase Complex from the Polychlorinated Biphenyls Degradation Pathway. *Biochemistry 50*, 8407−8416.

(11) Manjasetty, B. A., Powlowski, J., and Vrielink, A. (2003) Crystal structure of a bifunctional aldolase-dehydrogenase: sequestering a reactive and volatile intermediate. *Proc. Natl. Acad. Sci. U. S. A. 100*, 6992−6997.

(12) Miles, E. W., Rhee, S., and Davies, D. R. (1999) The molecular basis of substrate channeling. *J. Biol. Chem. 274*, 12193−12196.

(13) Huang, X., Holden, H. M., and Raushel, F. M. (2001) Channeling of substrates and intermediates in enzyme-catalyzed reactions. *Annu. Rev. Biochem. 70*, 149−180.

(14) Raushel, F. M., Thoden, J. B., and Holden, H. M. (2003) Enzymes with molecular tunnels. *Acc. Chem. Res. 36*, 539−548.

(15) Lee, S. J., Ko, J. H., Kang, H. Y., and Lee, Y. (2006) Coupled expression of MhpE aldolase and MhpF dehydrogenase in Escherichia coli. *Biochem. Biophys. Res. Commun. 346*, 1009−1015.

(16) Slayden, R. A., Jackson, M., Zucker, J., Ramirez, M. V., Dawson, C. C., Crew, R., Sampson, N. S., Thomas, S. T., Jamshidi, N., Sisk, P., Caspi, R., Crick, D. C., McNeil, M. R., Pavelka, M. S., Niederweis, M., Siroy, A., Dona, V., McFadden, J., Boshoff, H., and Lew, J. M. (2013) Updating and curating metabolic pathways of TB. *Tuberculosis (Edinb) 93*, 47−59.

(17) Baker, P., Hillis, C., Carere, J., and Seah, S. Y. (2012) Protein-protein interactions and substrate channeling in orthologous and

chimeric aldolase-dehydrogenase complexes. *Biochemistry 51*, 1942−1952.
(18) Wang, W., Baker, P., and Seah, S. Y. (2010) Comparison of two metal-dependent pyruvate aldolases related by convergent evolution: substrate specificity, kinetic mechanism, and substrate channeling. *Biochemistry 49*, 3774−3782.
(19) Baker, P., and Seah, S. Y. (2012) Rational design of stereoselectivity in the class II pyruvate aldolase BphI. *J. Am. Chem. Soc. 134*, 507−513.
(20) Wang, W., Mazurkewich, S., Kimber, M. S., and Seah, S. Y. (2010) Structural and kinetic characterization of 4-hydroxy-4-methyl-2-oxoglutarate/4-carboxy-4-hydroxy-2-oxoadipate aldolase, a protocatechuate degradation enzyme evolutionarily convergent with the HpaI and DmpG pyruvate aldolases. *J. Biol. Chem. 285*, 36608−36615.
(21) Liu, H., and Naismith, J. H. (2008) An efficient one-step site-directed deletion, insertion, single and multiple-site plasmid mutagenesis protocol. *BMC Biotechnol. 8*, 91.
(22) Nakashima, N., and Tamura, T. (2004) Isolation and characterization of a rolling-circle-type plasmid from Rhodococcus erythropolis and application of the plasmid to multiple-recombinant-protein expression. *Appl. Environ. Microbiol. 70*, 5557−5568.
(23) Shao, Z., Dick, W. A., and Behki, R. M. (1995) An improved *Escherichia coli*-Rhodococcus shuttle vector and plasmid transformation in Rhodococcus spp. using electroporation. *Lett. Appl. Microbiol. 21*, 261−266.
(24) Bradford, M. M. (1976) A rapid and sensitive method for the quantitation of microgram quantities of protein utilizing the principle of protein-dye binding. *Anal. Biochem. 72*, 248−254.
(25) Grochulski, P., Fodje, M. N., Gorin, J., Labiuk, S. L., and Berg, R. (2011) Beamline 08ID-1, the prime beamline of the Canadian Macromolecular Crystallography Facility. *J. Synchrotron Radiat. 18*, 681−684.
(26) Kabsch, W. (2010) Xds. *Acta Crystallogr. D Biol. Crystallogr. 66*, 125−132.
(27) McCoy, A. J., Grosse-Kunstleve, R. W., Adams, P. D., Winn, M. D., Storoni, L. C., and Read, R. J. (2007) Phaser crystallographic software. *J. Appl. Crystallogr. 40*, 658−674.
(28) Adams, P. D., Afonine, P. V., Bunkoczi, G., Chen, V. B., Davis, I. W., Echols, N., Headd, J. J., Hung, L. W., Kapral, G. J., Grosse-Kunstleve, R. W., McCoy, A. J., Moriarty, N. W., Oeffner, R., Read, R. J., Richardson, D. C., Richardson, J. S., Terwilliger, T. C., and Zwart, P. H. (2010) PHENIX: a comprehensive Python-based system for macromolecular structure solution. *Acta Crystallogr. D Biol. Crystallogr. 66*, 213−221.
(29) Emsley, P., Lohkamp, B., Scott, W. G., and Cowtan, K. (2010) Features and development of Coot. *Acta Crystallogr. D Biol. Crystallogr. 66*, 486−501.
(30) Delano, W. L. (2002) *The PyMOL Molecular Graphics System*, DeLano Scientific, San Carlos, CA.
(31) Capyk, J. K., Kalscheuer, R., Stewart, G. R., Liu, J., Kwon, H., Zhao, R., Okamoto, S., Jacobs, W. R., Jr., Eltis, L. D., and Mohn, W. W. (2009) Mycobacterial cytochrome p450 125 (cyp125) catalyzes the terminal hydroxylation of c27 steroids. *J. Biol. Chem. 284*, 35534−35542.
(32) Holm, L., and Rosenstrom, P. (2010) Dali server: conservation mapping in 3D. *Nucleic Acids Res. 38*, W545−549.
(33) Baker, P., Carere, J., and Seah, S. Y. (2011) Probing the Molecular Basis of Substrate Specificity, Stereospecificity, and Catalysis in the Class II Pyruvate Aldolase, BphI. *Biochemistry 50*, 3559−3569.
(34) Berka, K., Hanak, O., Sehnal, D., Banas, P., Navratilova, V., Jaiswal, D., Ionescu, C. M., Svobodova Varekova, R., Koca, J., and Otyepka, M. (2012) MOLEonline 2.0: interactive web-based analysis of biomacromolecular channels. *Nucleic Acids Res. 40*, W222−227.
(35) Moras, D., Olsen, K. W., Sabesan, M. N., Buehner, M., Ford, G. C., and Rossmann, M. G. (1975) Studies of asymmetry in the three-dimensional structure of lobster D-glyceraldehyde-3-phosphate dehydrogenase. *J. Biol. Chem. 250*, 9137−9162.
(36) Blanco, J., Moore, R. A., and Viola, R. E. (2003) Capture of an intermediate in the catalytic cycle of L-aspartate-beta-semialdehyde dehydrogenase. *Proc. Natl. Acad. Sci. U. S. A. 100*, 12613−12617.
(37) Demmer, U., Warkentin, E., Srivastava, A., Kockelkorn, D., Poetter, M., Marx, A., Fuchs, G., and Ermler, U. (2013) Structural basis for a bispecific NADP+ and CoA binding site in an archaeal malonyl-coenzyme A reductase. *J. Biol. Chem. 288*, 6363−6370.
(38) Ogasahara, K., Hiraga, K., Ito, W., Miles, E. W., and Yutani, K. (1992) Origin of the mutual activation of the alpha and beta 2 subunits in the alpha 2 beta 2 complex of tryptophan synthase. Effect of alanine or glycine substitutions at proline residues in the alpha subunit. *J. Biol. Chem. 267*, 5222−5228.
(39) Baker, P., Carere, J., and Seah, S. Y. (2012) Substrate Specificity, Substrate Channeling, and Allostery in BphJ: An Acylating Aldehyde Dehydrogenase Associated with the Pyruvate Aldolase BphI. *Biochemistry 51*, 4558−4567.
(40) Lei, Y., Pawelek, P. D., and Powlowski, J. (2008) A shared binding site for NAD+ and coenzyme A in an acetaldehyde dehydrogenase involved in bacterial degradation of aromatic compounds. *Biochemistry 47*, 6870−6882.
(41) Arnold, K., Bordoli, L., Kopp, J., and Schwede, T. (2006) The SWISS-MODEL workspace: a web-based environment for protein structure homology modelling. *Bioinformatics 22*, 195−201.